Theor Appl Climatol (2011) 103:387–399
DOI 10.1007/s00704-010-0305-8

ORIGINAL PAPER

Temperature variability in China in an ensemble simulation for the last 1,200 years

Dan Zhang · Richard Blender · Xiuhua Zhu · Klaus Fraedrich

Received: 18 January 2010 / Accepted: 4 June 2010 / Published online: 4 July 2010

Abstract Regional temperature anomalies in China during 800–2005 AD in an ensemble simulation with the atmosphere–ocean general circulation model ECHAM5/MPIOM subject to anthropogenic and natural forcings are compared to reconstructions. In a mutual assessment of three reconstructed data sets and two ensemble simulations with different solar forcings, a reconstructed data set and a simulated ensemble for weak solar variability are selected for further comparison. Temperature variability in the selected simulated and reconstructed data shows a continuous power spectrum with weak long-term memory. The simulation reveals weak long-term anomaly periods known as the Medieval Warm Period (MWP), the Little Ice Age (LIA), and the Modern Warming (MW) in the three considered regions: Northeast, Southeast, and West China. The ensemble spread yields an uncertainty of ±0.5°C in all regions. The simulated temperature varies nearly synchronously in all three regions, whereas reconstructed data hint to increased decadal variability in the West and centennial variability in the Northeast. Cold periods are found in 1200–1300 and in 1600–1900 AD in all regions. The coldest anomalies which are caused by volcanic eruptions in the beginnings of the thirteenth and the nineteenth centuries are only partly consistent with reconstructed data. After 1800, the annual cycle reduces in the Northeast and on the Tibetan plateau, whereas the eastern Pacific shows an enhanced summer–winter contrast.

D. Zhang · R. Blender · K. Fraedrich (✉)
Meteorological Institute, KlimaCampus, University of Hamburg,
Hamburg, Germany
e-mail: Klaus.Fraedrich@zmaw.de

D. Zhang
Institute of Geographic Sciences and Natural Resources Research,
Chinese Academy of Sciences,
Beijing, China

D. Zhang
Graduate School of the Chinese Academy of Sciences,
Beijing, China

X. Zhu · K. Fraedrich
Max Planck Institute for Meteorology, KlimaCampus,
Hamburg, Germany

1 Introduction

Information on the climate during the last millennium is known from reconstructions using proxy data and simulations with earth system models (ESMs). The variability of the Northern Hemispheric climate during the last millennium is commonly characterized by multi-century episodes with distinct temperature and humidity anomalies: the "Medieval Warm Period" (MWP, 900–1300 AD), the "Little Ice Age" (LIA, 1300–1850 AD), and the "Modern Warming" (MW, beginning in the nineteenth century). Due to substantial regional deviations, these climatic periods are not uniquely defined and describe a simplified view of past climate in the Northern Hemisphere (see Jones and Mann 2004 for a review and Jungclaus 2009 for a meeting summary).

These main climatic episodes are confirmed by temperature reconstructions for China (Wang et al. 1991, 2007; Yang et al. 2002, 2009; Ge et al. 2006; Qian et al. 2008). Regional reconstructions are available for Eastern China (Liu et al. 2005; Peng et al. 2009), the Huang He (Yellow River) and the Yangtze catchments (Ge et al. 2003; Zhang et al. 2008), West China (Holmes et al. 2009), and Tibet (Yang et al. 2003). Using proxy data in ten regions in China, Wang et al. (2007) claimed that the mean temperature in China varied in a range of about 1°C during the last

1,000 years. After 1400 AD, temperature decreased, with mean temperatures 0.6–0.9°C below present-day (Ge et al. 2003). Climate oscillations are found by Wang et al. (1991) in the annual mean temperature with periods of 200, 80, 30, and 22 years, which can be identified with the solar deVries (200y), Gleissberg (80y), and Hale cycles (22y); for an overview, see Tsiropoula (2003).

Several ESMs used for millennium simulations include a simplified atmosphere, for example simple energy balance models (Crowley et al. 2003), models without explicit atmospheric dynamics (CLIMBER; Bauer et al. 2003), or a quasigeostrophic atmosphere (ECBILT-CLIO-VECODE; Goosse et al. 2005). Complex ESMs simulate a coarse resolution dynamic atmosphere, the majority in T31 (~3.75°), for example CCSM2.01 (National Center for Atmospheric Research; Peng et al. 2009; Ammann et al. 2007), Goddard Institute for Space Studies-ER (Mann et al. 2009), and ECHO-G (ECHAM4/HOPE-G, May-Planck Institute for Meteorology; Zorita et al. 2004; Liu et al. 2005).

The advantages of complex ESMs are complete and dynamically consistent atmospheric and oceanic data sets and the assessment of the impact of different natural and anthropogenic forcings. The differences between millennium simulations are traced back to climate sensitivity, spin-up, and internal decadal variability by Goosse et al. (2005). Discrepancies between global reconstructions and two model simulations for the MWP–LIA difference were interpreted in terms of teleconnection patterns by Mann et al. (2009).

The comparison of simulated data obtained by dynamical ESMs with reconstructed data is necessary for the following reasons:

(a) Boundary conditions. Simulated climate variability depends to a large degree on the quality of reconstructed boundary conditions used in the model. One of the most important forcings is the solar irradiance for which the recent reconstruction by Krivova et al. (2007) assumes a smaller magnitude of variations than previous reconstructions (for example, Bard et al. 2000). The model output can be used to validate the reconstructed forcings.
(b) Reconstruction deficits. Reconstructed data suffer from several shortcomings: They depend to a large degree on statistical approaches and are possibly not dynamically consistent, the spatial coverage and the information are incomplete, and the uncertainty is poorly known. Model data can be useful to benchmark contradicting reconstructions.

Thus, the mutual assessment of dynamical earth system models and reconstructions is useful for the understanding of climate variability and the development of reliable models.

The aim of this publication is to derive the temperature anomalies in China during the last millennium on a regional basis. The approach begins with a mutual assessment of three reconstructed and two simulated temperature anomaly data sets in China. The simulated data are given by two full-forcing ensemble simulations for 800–2005 AD using the complex atmosphere–ocean general circulation model ECHAM5/MPIOM (Roeckner et al. 2003; Jungclaus and the COMSIMM Team 2009; Jungclaus et al. 2010). The two ensemble simulations are calculated using the state-of-the-art solar forcing reconstruction by Krivova et al. (2007) and a forcing reconstruction with higher variability (Bard et al. 2000). The uncertainty of the simulations is estimated by the ensemble spread which is a measure of the internal variability. In a first step, a reconstructed data set and the simulated ensemble for weak solar variability are selected for further analysis. The paper is organized as follows: In Section 2, a brief overview of reconstructed temperature in China during the last 1,200 years is given, and in Section 3, the model simulations and the experimental design are described. Section 4 includes the mutual assessment and the comparison of the simulated data with reconstructions in terms of the regional climate anomalies and centennial climate anomaly patterns. Section 5 concludes with a summary and a discussion.

2 Temperature reconstructions

The dominant climate variability observed in the Northern Hemisphere is confirmed by temperature reconstruction in China (see for example Yang et al. 2001, 2002; Wang et al. 2007). Data in the western part of China and on the Tibetan plateau are documented by Ge et al. (2006), Holmes et al. (2009), and Zhang et al. (2009). Ge et al. (2003) and Zhang et al. (2008) derived the winter temperature in eastern China with emphasis on the Huang He (Yellow River) and the Yangtze catchments. An outstanding deviation from the mean temperature in China is the absence of a distinct warming during the MWP in West China (Ge et al. 2006); instead, Xinjiang and the Qinghai–Tibet Plateau experienced a cold phase during the eleventh century (Wang et al. 2007). The temperature reconstructions in China during the last two millennia (Ge et al. 2010) reveal high consistency after 1500 AD for the five regions assessed (Northeast, Northwest, Southeast, Central East, and Tibet), whereas prior to 1500, large inconsistencies are found. In this publication, we focus on the data published by Wang et al. (2007) who present a detailed regional temperature reconstruction for the last 1,000 years (Northeast, North, East, South China, Taiwan, Central, Southwest, Northwest China, Xinjiang, and Qinghai–Tibet Plateau). This is based on a variety of proxy data (ice core, tree rings, stalagmites, peat, lake sediments, pollen, and historical records validated with instrumental observations made in the last 120 years). In Table 1, the reconstructed temperature anomalies during the last 1,200 years in the three regions, West, Northeast, and Southeast China, are summarized (Fig. 2); In 800–1000 AD, data of Ge et al. (2003) and Yang et al. (2002) are used; after 1000 AD, this follows Wang et al. (2007). The table shows three classes for the absolute anomalies: weak (<0.2°C), moderate (0.2–0.5°C), and large amplitudes (>0.5°C). The chronology is given by centennial means during three major climatic epochs, the MWP (900–1300 AD), the LIA (1300–1850 AD), and the MW (after 1850 AD). The temperature during the twentieth century was comparable to that in the MWP in East China.

3 Millennium simulation

The present analysis is based on the millennium experiments using the COSMOS-Atmosphere–Surface (Land)–Ocean-Biogeochemistry (ASOB) earth system model ("millennium run," Jungclaus 2009; Jungclaus and the COMSIMM Team 2009). The model includes the atmospheric model ECHAM5 (Roeckner et al. 2003), the ocean model MPIOM (Marsland et al. 2003), and modules for land vegetation (JSBACH; Raddatz et al. 2007) and ocean biogeochemistry (HAMOCC; Wetzel et al. 2006), which are coupled via the OASIS3 coupler. The carbon cycle is interactively simulated. ECHAM5 is run at T31 resolution (~3.75°) with 19 vertical levels and MPIOM at a horizontal grid spacing of about 3° with 40 unevenly spaced vertical levels.

Table 1 Summary of reconstructed centennial regional temperature anomalies in China in 800–2000 AD

	Years	China	Northeast	Southeast	West
	800–900	3	1	1/−2	1
MWP	900–1000	2	2	2/−1	1
	1000–1100	−1	2	1	−2
	1100–1200	1	2	1	−1
	1200–1300	1	3	1	−1
LIA	1300–1400	−1	3	1	−2
	1400–1500	−1	−1	−1	−1
	1500–1600	−1	−2	−1	−1
	1600–1700	−2	−2	−1	−2
	1700–1800	−1	−2	−1	1
MW	1800–1900	−1	−1	−2	2
	1900–2000	2	1	2	3

The anomalies are based on historical documents and proxy data from Wang et al. (2007) for 1000–2000 AD and Yang et al. (2002, 2003) and Ge et al. (2003) for 800–1000 AD. The classes are defined as −3 (≤0.5°C), −2 (−0.5…−0.2), −1 (−0.2…0), 1 (0…0.2), 2 (0.2…0.5), and 3 (>0.5); ambiguous proxies before 1000 AD by (/)

MWP Medieval Warm Period, *LIA* Little Ice Age, *MW* Modern Warming

The model is forced by reconstructions of (1) total solar irradiance (TSI), (2) volcanic forcing considering aerosol optical depth (AOD) and effective radius distribution, (3) land use change, and (4) anthropogenic greenhouse gases and aerosols. The TSI is based on data reconstructed by Krivova et al. (2007). It combines sun-spot observations starting back in the seventeenth century and variations of atmospheric C14 concentrations derived from tree rings. The TSI time series exhibits low long-term variability of about 0.1% of the standard TSI value of 1367 Wm^{-2} (given by the difference between present-day and Maunder minimum).

The volcanic effects are taken into account in a data set of AOD and effective radius for 10-day time steps and split into four equal area segments (30–90° N, 0–30° N, 30–0° S, 90–30° S). Growth and decay time for each eruption is calibrated and fitted to recent observations. The data set includes information about mean particle radius evolution vs. time, a feature particularly important for large eruptions (for details, see Crowley et al. 2008). Timmreck et al. (2009) have shown for the 1258 eruption that a shift of the volcanic aerosol size distribution toward larger particles reduces the cooling effect and improves the consistency with temperature reconstructions.

Anthropogenic land use change prior to 1700 is reconstructed by Pongratz et al. (2008) and after 1700 by Foley et al. (2003). In China where crop areas were already large at 800 AD, natural vegetation is almost completely replaced by agricultural land use after 1700 in Southeast China.

The analysis uses two ensemble experiments, a first with five members forced by weak (0.1%) and a second with three members forced by intense solar forcing variability (0.25%); the remaining natural and anthropogenic forcings are identical and cover the period from 800 to 2005 AD (Bard et al. 2000; Jungclaus et al. 2010). The different initial conditions for the ensemble members are derived from a 3,000-year control integration forced by constant conditions for 1860. If not indicated otherwise, the ensemble mean is analyzed in this publication.

The comparison of the impact of different forcing mechanisms in the millennium experiments (Jungclaus et al. 2010) yields that the variability is dominated by volcanic eruptions decreasing the net short wave radiation at the top of the atmosphere (Fig. 1a, incoming solar radiation reduced by cloud and aerosol reflection for the weak solar irradiance variability of 0.1%). The most severe eruption occurred in 1258 (Stothers 1984), presumably in the lower latitudes, and the second most severe was the Tambora eruption in 1815. The Maunder minimum of solar activity (1645–1715) is barely detectable, while the Dalton minimum

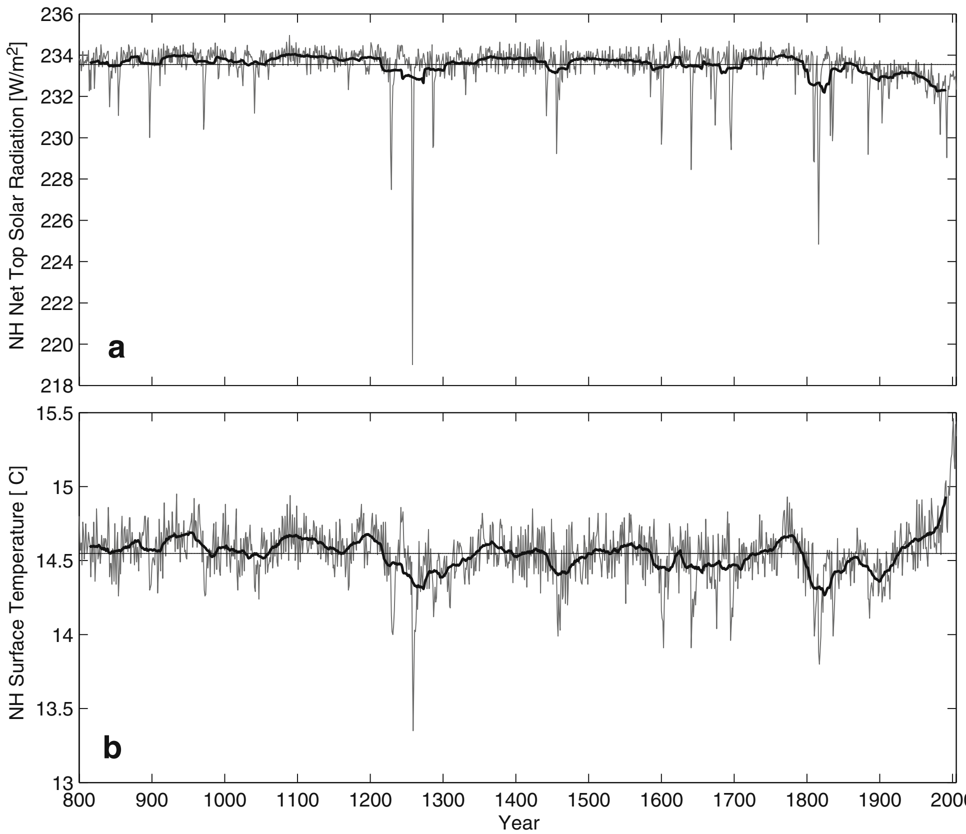

Fig. 1 Northern Hemispheric annual means of net shortwave radiation at the top of the atmosphere (**a**) and surface temperature (**b**); 30-year running means are indicated (*bold*)

(1790–1830) comprises a series of volcanic eruptions (Cole-Dai et al. 2009).

The ensemble mean of the Northern Hemispheric mean surface temperature (Fig. 1b) shows distinct long-term climate anomalies. Decadal cooling periods are found after volcanic eruptions in 1258 (unknown volcano) and 1815 (Tambora), respectively; the latter period coincides with the Dalton minimum (1790–1830). A warm period in 1100–1200 may be associated with the MWP, and an intermittent cool period during 1400–1700 corresponds to the LIA. After 1900, the modern warming commenced. The cooling of −0.1°C during the LIA in the Northern Hemisphere is much less pronounced than the reconstructed range, between −0.6°C and −0.3°C (Mann et al. 2008). Volcanic eruptions are the most efficient impacts on surface temperature during the pre-industrial era.

4 Simulated temperature

The first aim is to compare three reconstructed near surface temperature data sets with two simulations obtained for different solar forcing reconstructions in order to select a reconstruction and a simulated data set which agree within an uncertainty given by the internal climate variability. This mutual assessment, which is based on the mean temperature in China, includes a spectral analysis to validate the data using information on low-frequency variability detected in previous analyses. The main part of the analysis is a comparison of regional climate anomalies in China in the selected reconstructed and simulated data sets.

(a) Mutual assessment of solar irradiance forcings and different reconstructions

An ensemble simulation with increased solar irradiance variability (see Section 3) is included and both simulations are compared with three reconstructed data sets (Ge et al. 2003; Yang et al. 2002; Wang et al. 2007). The comparison which includes a spectral analysis yields considerable differences between reconstructed data and gives some hint to the assessment of the forcing.

(b) Regional temperature and ensemble spread

For a comparison with reconstructions, China is divided into three regions (Fig. 2): Northeast, Southeast, and West China. The uncertainty of the ensemble experiments is derived by the spread of temperature extremes on decadal timescales. The time series are compared with reconstructed data.

(c) Centennial temperature anomaly patterns and annual cycle

For a detailed geographical comparison, the time span of the model simulation is split into bicentennial time bins

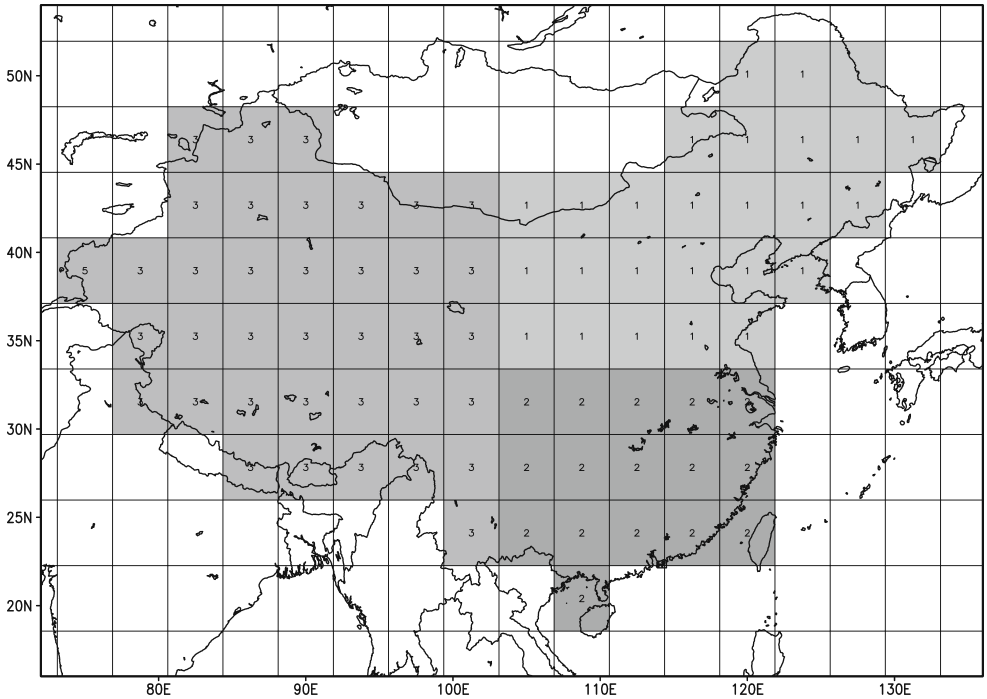

Fig. 2 Regions in China marked by grid points in the ECHAM5 T31 model simulation (*1* Northeast China, *2* Southeast China, *3* West China)

beginning with the ninth century up to the present day. Particular periods are assessed for a comparison with the climatology merged by Wang et al. (2007). The model results are used to retrieve the change of the annual cycle during the past 1,200 years.

4.1 Mutual assessment of solar irradiance forcings and different reconstructions

Three reconstructions of the mean temperature in China are compared with the ensemble means in simulations which differ with respect to the variability of the solar forcing (Fig. 3; see Section 3). The reconstructed temperature anomalies by Yang et al. (2002) (decadal means in China) and Ge et al. (2003) (30-year winter means in East China with decadal means in 960–1100 and after 1500) show large centennial variability of the order of 1°C, which are far beyond the reconstructions by Wang et al. (2007) (decadal means, after 1000 AD) as well as the model uncertainty. For example, in Yang et al. (2002), the mean temperature in 800–900 is 0.6°C and shows −0.6°C in 1400–1700. In Ge et al. (2003), the temperature anomaly reaches more than +1°C for decades in the thirteenth century and falls below −0.6°C in 1800–1900. The mutual comparison of the simulated and the reconstructed data indicates that the reconstructions by Wang et al. (2007) are reconcilable with the simulations (see Section 4.2).

The variability of these data (standard deviation 0.27°C), however, is too large to provide an assessment of both simulations. The 0.25% variability simulation reveals larger anomalies and in particular a warmer MWP (0.1°C) and a cooler LIA (−0.07°C) compared to the 0.1% variability experiments. Compared to the 1960–1990 mean, the Maunder minimum (1645–1715) is −0.34°C (−0.35°C) colder in the 0.1% (0.25%) variability simulations. Therefore, based on the data by Wang et al. (2007), we cannot decide whether the solar forcing with higher solar variability (0.25%) is preferable to the forcing with weak variability (0.1%).

Since reconstructed and simulated data indicate considerable differences in low-frequency variability (Fig. 3), the comparison is complemented by spectral analysis. In the last years, several investigations could show that interannual temperature variability is dominated by power laws, $S(f) \sim f^{-\beta}$, in wide ranges of timescales (Fraedrich and Blender 2003; Huybers and Curry 2006). Thus, climate variability is present on all timescales with a continuous background superimposed with oscillations or cycles. For positive exponents, $\beta > 0$, this long-term memory is explained by the thermal inertia of subsystems, mainly the ocean. Long-term memory is also found in a long-term simulation of the hydrological cycle with the coupled model ECHAM5/MPIOM in China (Blender and Fraedrich 2006).

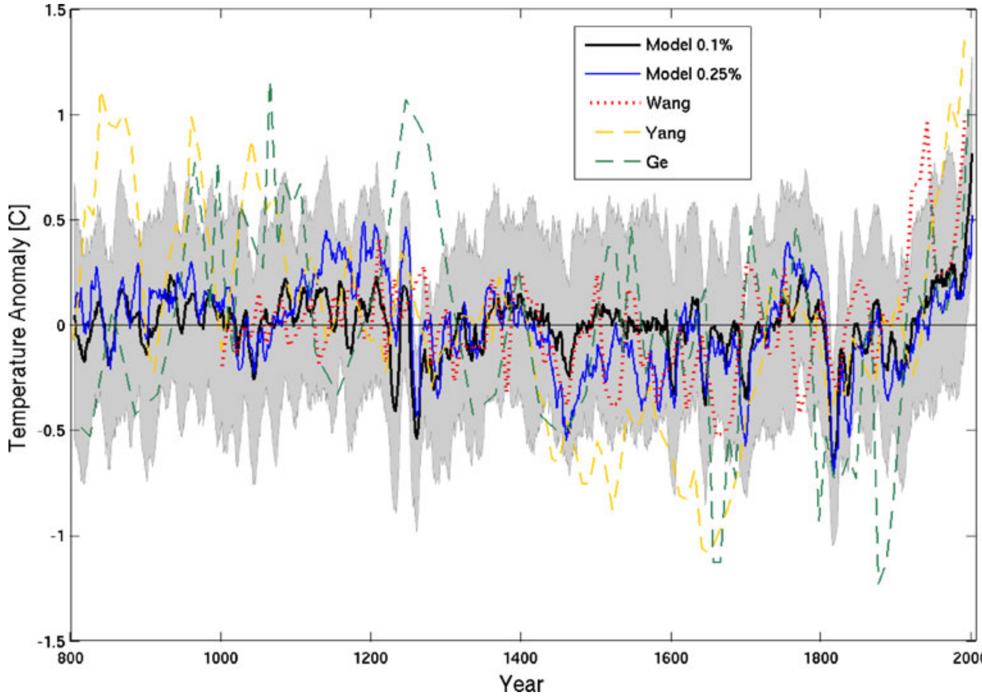

Fig. 3 Temperature anomalies in China: two simulations with 0.1% (*black*/*solid*) and 0.25% (*blue*/*solid*) solar irradiance variability amplitude, respectively, and reconstructions by Wang et al. (2007) (*dotted*/*red*), Yang et al. (2002) (*dashed*/*yellow*), and Ge et al. (2003) (*dashed*/*green*). The ensemble spread (from the 0.1% amplitude simulation) is indicated by the 11-year running means of simulated minimum and maximum anomalies in the ensemble (*shaded*)

The simulated temperature (with annual resolution) shows a nearly continuous power spectrum with an exponent $\beta \approx 0.5$, which is valid in the whole accessible frequency range from annual to several centuries (Fig. 4a). The single deflection is an increase in power within the frequency range corresponding to 3–4 years, which can be attributed to ENSO. Further periodic or quasi-periodic variability contributions are not simulated (see for example Wang et al. (1991)). The ensemble with the increased solar irradiance variability (0.25%, not shown) reveals a power spectrum with the same scaling and exponent. The exponent β is determined by detrended fluctuation analysis (Hurst exponent $\alpha = 0.75$; Fraedrich and Blender 2003). Note that in instrumental records and long-term simulations, smaller values of $\beta \approx 0.2 \ldots 0.4$ are found on land on timescales up to centuries (Fraedrich and Blender 2003). In climate simulations, long-term memory is caused by dynamic ocean models which show a variety of spectra (Zhu et al. 2006).

The power spectrum of the reconstructed decadal mean temperature (Wang et al. 2007) shows scaling with the same exponent $\beta \approx 0.5$ (Fig. 4b). Thus, the simulated and the reconstructed temperature time series indicate the same type of long-term memory. The power spectra of the reconstructed temperature time series proposed by Yang et al. (2002) and Ge et al. (2003) in Fig. 4c confirm the high low-frequency variability observed (Fig. 3). Both spectra increase steeply for low frequencies with a spectrum that can be roughly estimated as $S(f) \sim 1/f^2$; hence, $\beta \approx 2$. This result provides further evidence that the reconstruction by Wang et al. (2007) is in agreement with the model simulation.

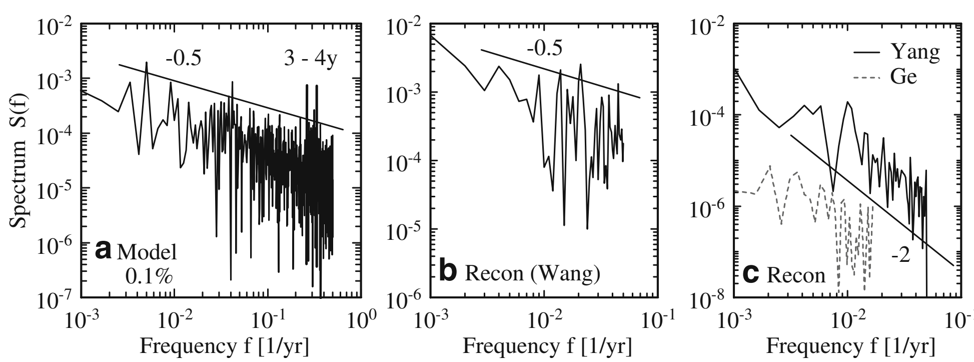

Fig. 4 Power spectra of the mean temperature in China: **a** simulated (0.1% amplitude of the solar irradiance variability), **b** reconstructions by Wang et al. (2007), and **c** by Yang et al. (2002) (*solid*) and Ge et al. (2003) (*dashed*). *Solid lines* indicate scaling $S(f) \sim f^{-\beta}$. In **a**, the 3- to 4-year ENSO cycle is evident

In summary, we conclude that given that the reconstruction of the solar irradiance with 0.1% variability is considered as a state-of-the-art (see Krivova et al. 2007), there is no need to deviate from this suggestion and that this forcing intensity is appropriate for millennium simulations.

4.2 Regional temperature and ensemble spread

Temperature time series for China and three regional averages (Northeast, Southeast, and West) are compared with the reconstruction by Wang et al. (2007). The uncertainty of the simulation is estimated by the minima and maxima in the five-member ensemble. The mean temperature in China (Fig. 5a) is above normal in 900–1200 and below average during 1200–1300 and 1800–1900 AD. An anomalously cold and persistent LIA is hardly distinguishable. This is comparable to the simulation by Peng et al. (2009). The cool periods during the thirteenth and nineteenth centuries are associated with sequences of the most intense volcanic eruptions in 1258 and in 1815 (Tambora). After that, the cold temperature anomalies recover on decadal timescale, which is attributed to the ocean heat uptake in a coupled ensemble experiment (Stenchikov et al. 2009). According to Cole-Dai et al. (2009), 1810–1819 was the coldest period during the last 500 years. A short cooling period appears at the end of the nineteenth century, which is most dominant in the Northeast (Fig. 5b). A possible reason for this cooling is a sequence of volcanic eruptions (Krakatau in 1883, Santa Maria and Mount Pelée in 1902, and Novarupta in 1912). The Maunder minimum in 1645–1715 is related to a centennial period with a weak cooling, while the Dalton minimum in 1790–1830 is marked by a strong cooling for roughly two decades. The dominant temperature change occurs during the MW in the twentieth century.

Regional averages of temperature in Northeast, Southeast, and West China reveal major consistent long-term anomalies determined with respect to the total simulation period (Fig. 5b–d). All regional temperature anomalies vary within a corridor of ±0.5°C. The differences between regional temperatures, however, are much weaker than between reconstructed anomalies. The most remarkable differences are in the Northeast with a distinct reconstructed warming in 1000–1400 AD and a cooling from 1400–1800 AD; but much weaker anomalies are found in the Southeast. The reconstructed temperature anomalies in the Northeast are characterized by centennial variability, whereas decadal variability dominates in the West.

4.3 Centennial temperature anomaly patterns and annual cycle

In this section, the simulated ensemble mean is first compared with the reconstructed temperature anomalies

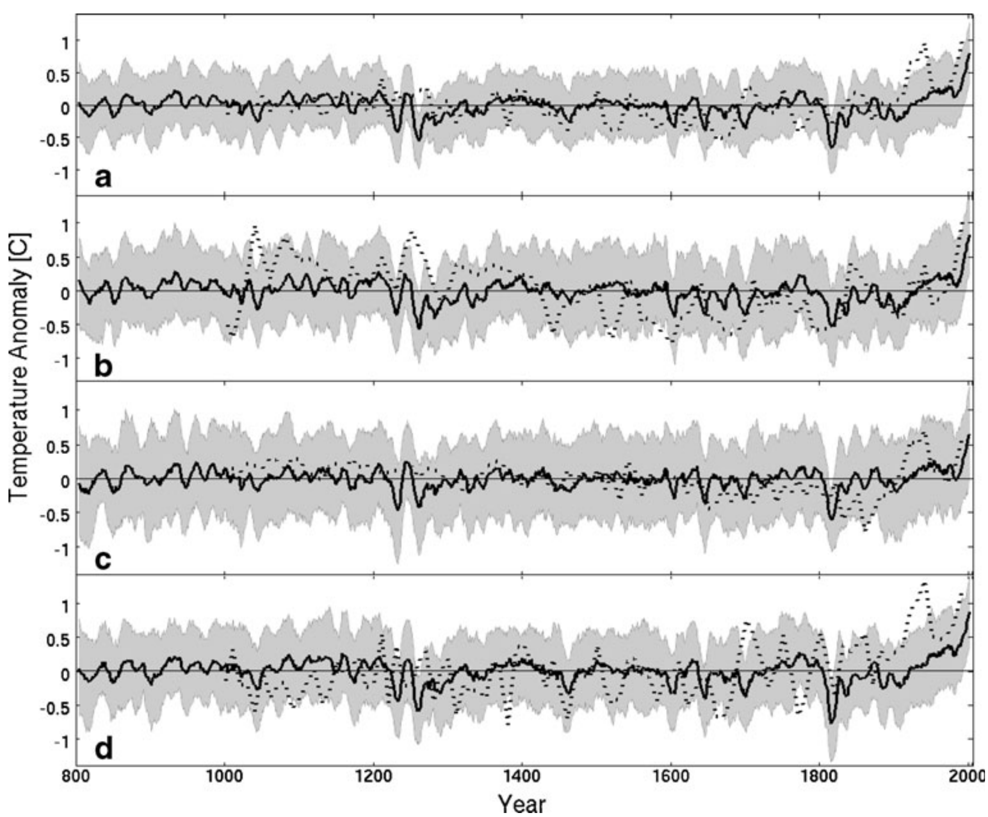

Fig. 5 Temperature anomalies in China (**a**), Northeast (**b**), Southeast (**c**), and West (**d**). Simulations: ensemble means (*bold*) and spread as 11-year running means of minimum and maximum (*shaded*). Reconstruction (*dotted*) by Wang et al. (2007). Simulated (reconstructed) anomalies are with respect to the 800–2005 (1000–2000) mean

patterns for periods given by Wang et al. (2007), which is complemented by a bicentennial decomposition of temperature anomalies during 800–2000 AD.

4.3.1 Comparison with centennial temperature reconstructions

Wang et al. (2007) present a geographic overview of climate anomalies for the last millennium considering distinct periods: (a) 1041–1140, (b) 1171–1270, (c) 1601–1700, and (d) 1781–1880 and the shorter periods (e) 1951–2000 and (f) 1991–2000. This summary of long-term mean temperatures is an apt compilation for the assessment of the simulation. For ease of comparison, the anomalies of the near surface temperature are determined for the corresponding periods (all anomalies are relative to the mean in the total range 800–2005). The main findings are summarized as follows (Fig. 6, compare Fig. 5 in Wang et al. 2007 and Fig. 2 in Mann et al. 2009):

(a) 1041–1140: The model shows a moderate warming of the order of 0.1°C for East Asia, whereas in the reconstructions, the western part is colder than average and the East is distinctly warmer, up to 0.4°C warmer in the Northeast (Table 1 and Wang et al. 2007; compare Mann et al. 2009).
(b) 1171–1270: The simulations reveal a negative anomaly in West China which agrees with reconstructions by Wang et al. (2007). The reconstructed warming in the Northeast is not found in the simulation.
(c) 1601–1700: This century is the coldest period during the LIA (for the Northern Hemisphere, see Mann et al. 2009) which is captured as well in the reconstruction by Wang et al. (2007). The simulated temperature anomaly pattern agrees with the reconstructions; in the Southeast where a negligible anomaly is reconstructed, the simulated cooling is not significant.
(d) 1781–1880: The simulation reveals a persistent LIA with even lower temperature anomalies than during 1601–1700. This century includes the Dalton minimum and in particular the extreme cold decade 1810–1819 (Cole-Dai et al. 2009). The simulated cold century deviates from the reconstructions by Wang et al. (2007), mainly in the West.
(e) 1951–2000 and (f) 1991–2000: These periods show the highest temperature during the last millennium (up to 0.9°C, significant in almost all regions).

In summary, a distinct medieval warming in China is found in the simulation until 1140 AD; this is terminated by a cooling during 1170–1270 (in the reconstructions by Wang et al. 2007, the medieval warming persists until 1270). The LIA persists until the nineteenth century. Before 1900, the absolute values of the simulated temperature anomalies are lower than in the reconstructions (±0.2°C compared to ±0.4°C).

4.3.2 Bicentennial temperature patterns

The simulated temperature anomalies are assessed by means for adjacent bicentennial periods (800–1000, 1000–1200, etc.) to obtain a complete overview of the climate evolution in China (Fig. 7).

(a) 800–1200: During this period, which is considered as the warmest during the last two millennia in the Northern Hemisphere (Mann et al. 2008), moderate warming prevailed in China (up to +0.1°C). Deviations from this are weak and limited to a few regions. In 800–1200, significance is restricted to the Northeast, in 1000–1200 also in the northwest. Recent reconstructions of Mann et al. (2009) find a warming up to +0.5°C in Southeast Asia.
(b) 1200–1800: A complete cooling is the most distinct feature of these centuries (significant in the West and in the Southeast China). In 1200–1400 and 1600–1800, the cold anomalies below −0.08°C are significant. The simulated LIA cooling is interrupted during 1400–1600 in Tibet and the Northeast when the LIA prevailed in the Northern Hemisphere (Mann et al. 2008). A warming is reconstructed by Mann et al. (2009) for 1400–1700 in Southeast Asia.
(c) 1800–2000: The model shows a cold northeast and a warm southeast China. In the northeast, the cold anomalies at the beginning of the nineteenth century (Fig. 6d) compensate for the warming in the twentieth century in the North (Fig. 7f).

4.3.3 Annual cycle

The climate evolution is accompanied by a considerable change of the annual cycle (Fig. 8, note that this figure shows anomalies of summer minus winter temperatures with respect to the total simulated period). During 800–1200 (MWP) until the advent of the LIA, the annual cycle shows a pronounced land–sea contrast with largest differences on the Tibetan plateau. Within 1200–1400, the annual cycle begins to weaken and the anomalies reverse in Central China. During the cold period in 1400–1800, the annual cycle reduces further (except in the Northwest) and reverses on the Tibetan plateau. After 1800, a severe reduction of the annual cycle in the North and on the Tibetan plateau is found, whereas the eastern Pacific shows an enhanced summer–winter contrast. Thus, the annual cycles during the modern and the medieval warming differ considerably. The most probable reason is the anthropogenic aerosol load which increased during the twentieth century.

5 Summary and discussion

The near surface temperature data in a 1,200-year climate simulation (millennium run) are compared to reconstructed regional temperature records in China. The millennium run

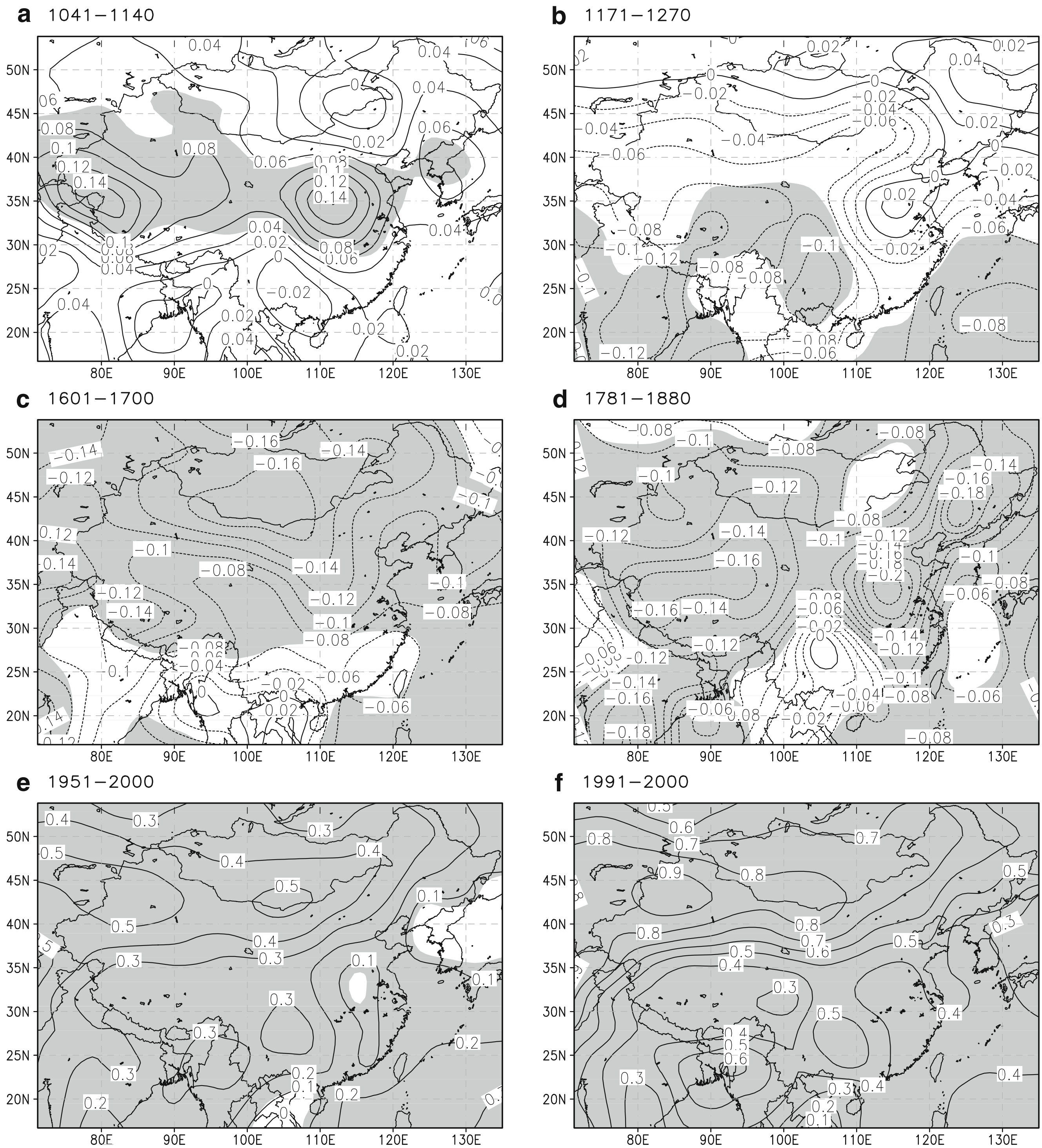

Fig. 6 Simulated temperature anomalies during the periods as indicated (with respect to the overall mean in 800–2005, compare with Fig. 5 of Wang et al. (2007)); areas with 95% significance are *shaded*

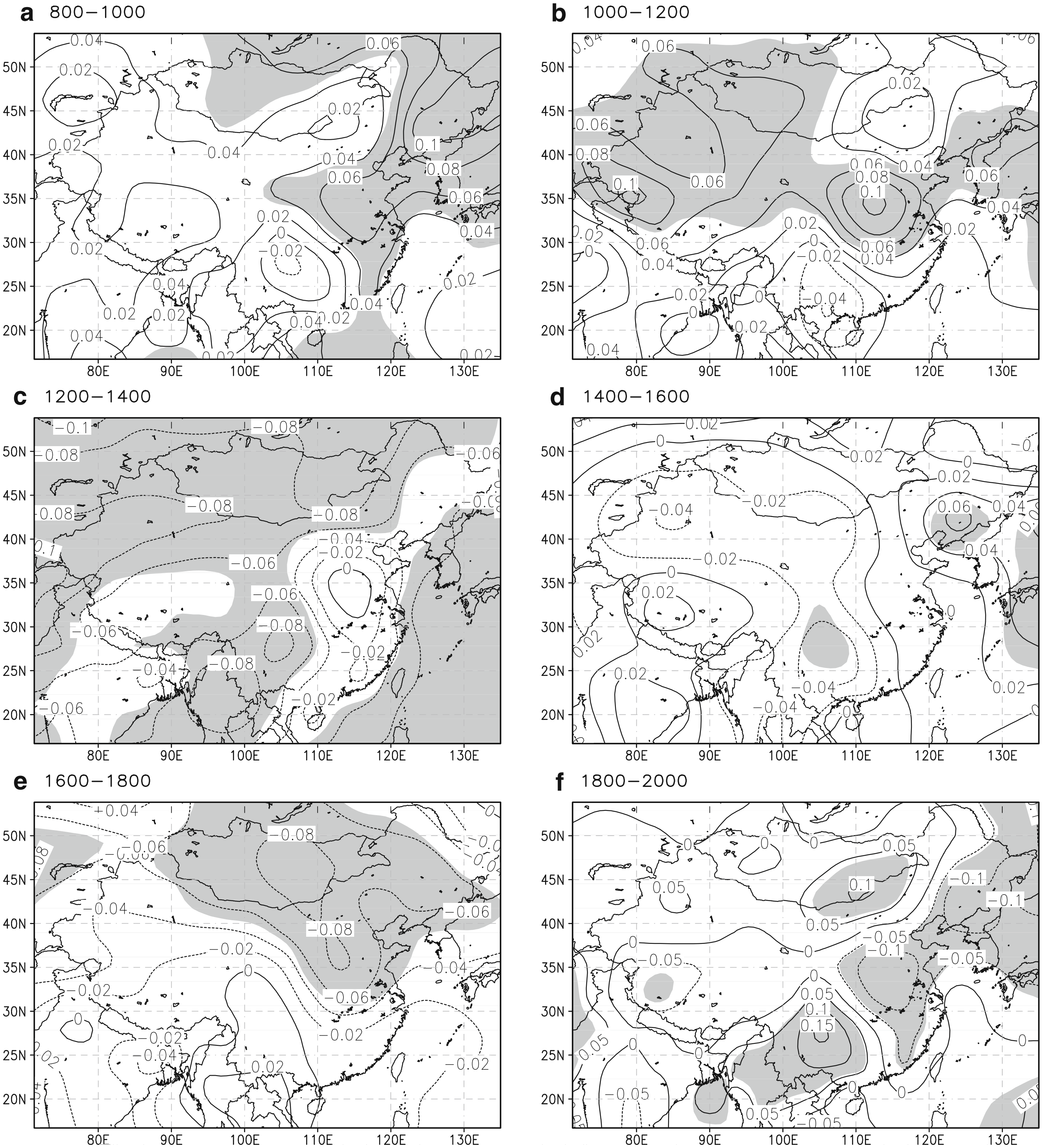

Fig. 7 Simulated temperature anomalies as bicentennial means (with respect to the overall mean in 800–2005); areas with 95% significance are *shaded*

is designed as an ensemble of simulations with the atmosphere ocean general circulation model ECHAM5/MPIOM including modules for land vegetation and ocean biogeochemistry. The model is forced by reconstructed TSI, volcanic forcing (by aerosol optical depth and effective radius distribution), land use change, and anthropogenic greenhouse gases and aerosols.

A mutual comparison of simulated and three reconstructed data sets indicates that the reconstructions by Wang et al. (2007) are reconcilable with the simulations obtained

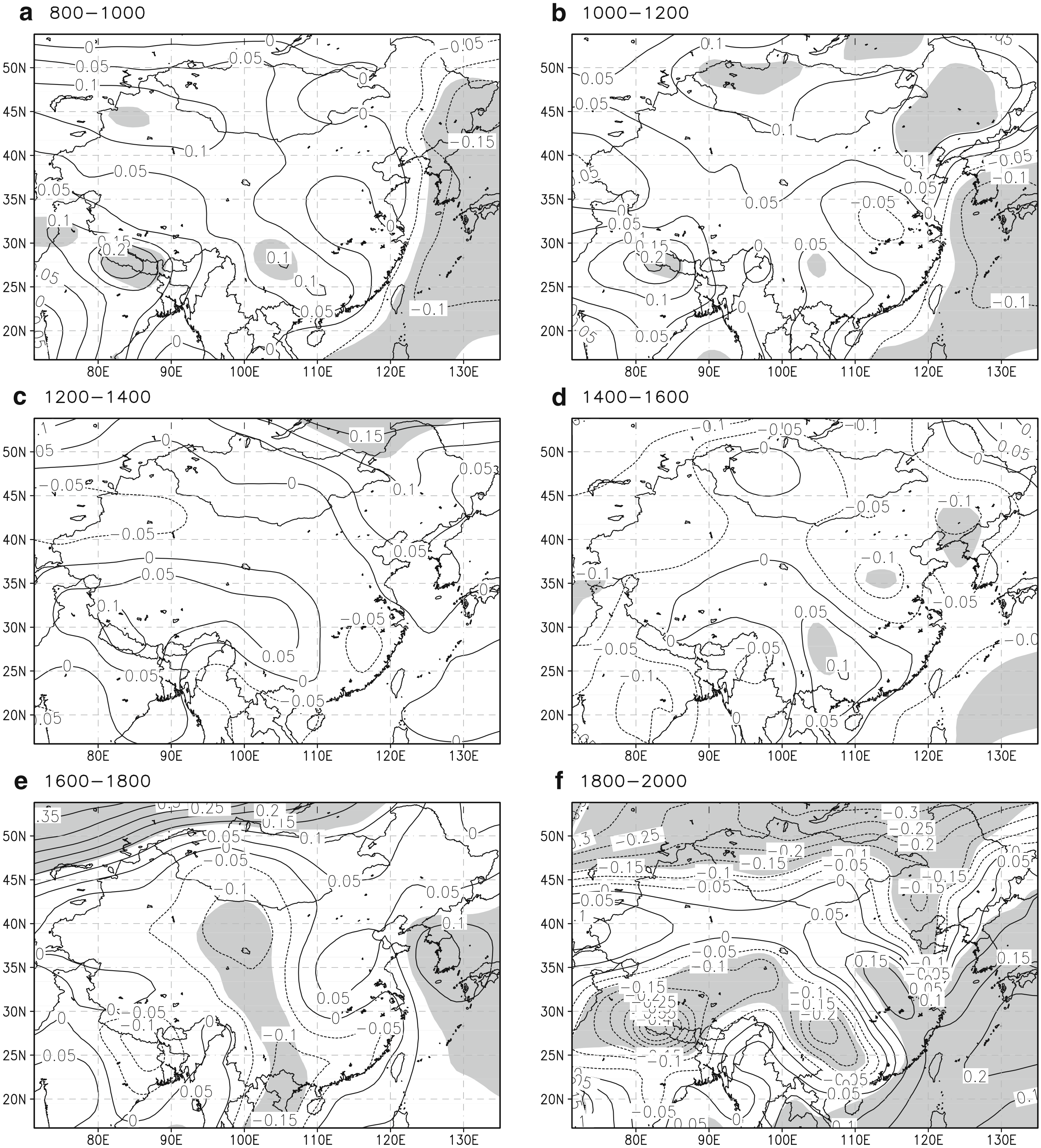

Fig. 8 Simulated annual cycle (defined as summer minus winter temperature) as bicentennial means. The mean annual cycle in 800–2005 is subtracted and areas with 95% significance are *shaded*

with the solar irradiance by Krivova et al. (2007) with a variability amplitude of 0.1%. The long-term anomalies of other reconstructions are beyond the uncertainty given by the simulations. The low-frequency variability of the simulated mean temperature in China reveals a power law scaling in the power spectrum, $S(f) \sim f^{-\beta}$ with $\beta{\approx}0.5$, indicating stationary long-term memory (obtained for both the 0.1% and the 0.25% forcing amplitudes). This agrees with the variability of the reconstructed mean temperature in China by Wang et al. (2007), whereas other reconstructions reveal non-stationary power spectra with $\beta{\approx}2$.

The simulated Northern Hemispheric means show long-term warming and cooling periods corresponding to the MWP in 900–1300, the LIA in 1300–1850, and the MW after 1850. Volcanic eruptions are the most efficient external forcing (Jungclaus and the COMSIMM Team 2009). The spread within the ensemble simulations yields the uncertainty ±0.5°C of the dynamic reconstruction.

The model simulations are compared to regional temperature reconstruction with decadal and centennial temporal resolution (Wang et al. 2007). Deviations from the reconstructions are: During the eleventh century, the model shows a moderate warming in China, whereas reconstructions indicate a zonal temperature contrast with a cooler western and a warmer eastern part. A further discrepancy is found in the thirteenth century when simulations are too cool in the West and the Northeast (in the Southeast, the simulations agree with reconstructions). During the LIA, the simulated temperature anomaly agrees with reconstructions in the West and the Northeast. The annual cycle during the MWP was stronger on land but weaker on the East Pacific compared to the last two centuries.

The present analysis reveals the following results: (1) The comparison of the temperature anomalies in China obtained in the model simulation with reconstructed data demonstrates that the simulation with weak 0.1% solar irradiance variability is reconcilable with the reconstructions by Wang et al. (2007). (2) Simulated regional temperature anomalies show high interannual variability on decadal timescales with volcanic eruptions as the dominant signature. (3) The uncertainty of the simulated mean temperature is of the order of ±0.5°C. (4) The power spectra of the simulated and reconstructed mean temperature in China agree and indicate stationary long-term memory, while periodicities apart from ENSO (3–4 years) are not simulated. (5) The land–sea contrast of the annual cycle changed sign during the last millennium.

Acknowledgments We like to thank Johann Jungclaus, Martin Claußen, and the Millennium Consortium at the Max-Planck Institute and at the University of Hamburg for providing the simulated data and for stimulating discussions. We are grateful to Wang Shao-Wu (Peking University, Beijing) for the reconstructed temperature time series. DZ acknowledges the support for the visit at Hamburg by the Institute of Geographic Sciences and Natural Resources Research (Chinese Academy of Sciences) and the Graduate School of the Chinese Academy of Sciences. The suggestions of the two anonymous reviewers helped improve the paper considerably.

References

Ammann CM, Joos F, Schimel DS, Otto-Bliesner BL, Tomas RA (2007) Solar influence on climate during the past millennium: results from transient simulations with the NCAR climate system model. PNAS 104:3713–3718

Bard E, Raisbeck G, Yiou F, Jouzel J (2000) Solar irradiance during the last 1200 years based on cosmogenic nuclides. Tellus 52B:985–992

Bauer E, Claussen M, Brovkin V (2003) Assessing climate forcings of the Earth system for the past millennium. Geophys Res Lett 30:1276. doi:10.1029/2002GL016639

Blender R, Fraedrich K (2006) Long term memory of the hydrological cycle and river runoffs in China in a high resolution climate model. Int J Climatol 26:1547–1565

Cole-Dai J, Ferris D, Lanciki A, Savarino J, Baroni M, Thiemens MH (2009) Cold decade (AD 1810–1819) caused by Tambora (1815) and another (1809) stratospheric volcanic eruption. Geophys Res Lett 36:L22703

Crowley TJ, Baum SK, Kim KY, Hegerl GC, Hyde WT (2003) Modeling ocean heat content changes during the last millennium. Geophys Res Lett 30:1932. doi:10.1029/2003GL017801

Crowley TJ, Zielinski G, Vinther B, Udisti R, Kreutz K, Cole-Dai J, Castellano E (2008) Volcanism and the Little Ice Age. PAGES News 16:22–23

Foley JA, Delire C, Ramankutty N, Snyder P (2003) Green surprise? How terrestrial ecosystems could affect Earth's climate. Front Ecol Environ 1:38–44

Fraedrich K, Blender R (2003) Scaling of atmosphere and ocean temperature correlations in observations and climate models. Phys Rev Lett 90:108501

Ge QS, Zheng JY, Fang XQ, Man ZM, Zhang XQ, Zhang PY, Wang WC (2003) Winter half-year temperature reconstruction for the middle and lower reaches of the Yellow River and Yangtze River, China, during the past 2000 years. The Holocene 13:933–940. Data from: East-Central China Winter Half-year Temperature Reconstruction, IGBP PAGES/World Data Center for Paleoclimatology. Data Contribution Series #2003-090. NOAA/NGDC Paleoclimatology Program, Boulder CO, USA

Ge QS, Wang SB, Zheng JY (2006) Reconstruction of temperature series in China for the last 5000 years. Prog Nat Sci 16:838–845 (in Chinese)

Ge QS, Zheng JY, Hao ZX, Shao XM, Wang W-C, Luterbacher J (2010) Temperature variation through 2000 years in China: an uncertainty analysis of reconstruction and regional difference. Geophys Res Lett 37:L03703

Goosse H, Renssen H, Timmermann A, Bradley RS (2005) Internal and forced climate variability during the last millennium: a model-data comparison using ensemble simulations. Quatern Sci Rev 24:1345–1360

Holmes JA, Cook ER, Yang B (2009) Climate change over the past 2000 years in Western China. Quatern Int 194:91–107

Huybers P, Curry W (2006) Links between annual, Milankovitch and continuum temperature variability. Nature 441:329–332

Jones PD, Mann ME (2004) Climate over past millennia. Rev Geophys 42(RG2002):1–42. doi:10.1029/2003RG000143

Jungclaus JH (2009) Lessons from the past millennium. Nat Geosci 2:468–470

Jungclaus J, the COMSIMM Team (2009) Ensemble simulations of the last millennium using an earth system model including an interactive carbon cycle. Geophysical Research Abstracts 11, EGU General Assembly 2009-4043

Jungclaus JH, Lorenz SJ, Timmreck C, Reick CH, Brovkin V, Six K, Segschneider J, Giorgetta MA, Crowley TJ, Pongratz J, Krivova NA, Vieira LE, Solanki SK, Klocke D, Botzet M, Esch M, Gayler V, Haak H, Raddatz TJ, Roeckner E, Schnur R, Widmann H, Claussen M, Stevens B, Marotzke J (2010) Climate and carbon-cycle variability over the last millennium. Clim Past Discuss 6:1009–1044

Krivova NA, Balmaceda L, Solanki SK (2007) Reconstruction of solar total irradiance since 1700 from the surface magnetic flux. Astron Astrophys 467:335–346

Liu J, von Storch H, Chen X, Zorita E, Zheng J, Wang S (2005) Simulated and reconstructed winter temperature in the eastern China during the last millennium. Chin Sci Bull 50:2872–2877

Mann ME, Zhang Z, Hughes MK, Bradley RS, Miller SK, Rutherford S, Ni F (2008) Proxy-based reconstructions of hemispheric and global surface temperature variations over the past two millennia. PNAS 105:13252–13257

Mann ME, Zhang Z, Rutherford S, Bradley RS, Hughes MK, Shindell D, Ammann C, Faluvegi G, Ni F (2009) Global signatures and dynamical origins of the little ice age and medieval climate anomaly. Science 326:1256–1260

Marsland S, Haak H, Jungclaus J, Latif M, Röske F (2003) The Max-Planck-Institute global ocean/sea ice model with orthogonal curvilinear coordinates. Ocean Model 5:91–127

Peng YB, Xu Y, Jin L (2009) Climate changes over eastern China during the last millennium in simulations and reconstructions. Quatern Int 208:11–18. doi:10.1016/j.quaint.2009.02.013

Pongratz J, Reick C, Raddatz T, Claussen M (2008) A reconstruction of global agricultural areas and land cover for the last millennium. Global Biogeochem Cycles 22:GB3018. doi:10.1029/2007GB003153

Qian W, Ding T, Fu J, Lin X, Zhu Y (2008) Review on the data application and climate variability in China for various timescales. Adv Climate Change Res Suppl 4:1–6

Raddatz TJ, Reick CJ, Knorr W, Kattge J, Roeckner E, Schnur R, Schnitzler KG, Wetzel P, Jungclaus JH (2007) Will the tropical land biosphere dominate the climate-carbon cycle feedback during the 21st century? Climate Dyn 29:565–574

Roeckner E, Bäuml G, Bonaventura L, Brokopf R, Esch M, Giorgetta M, Hagemann S, Kirchner I, Kornblueh L, Manzini E, Rhodin A, Schlese U, Schulzweida U, Tompkins A (2003) The atmospheric general circulation model ECHAM5. Part I: model description. Max Planck Institute for Meteorology, Report 349, p 127

Stenchikov G, Delworth TL, Ramaswamy V, Stouffer RJ, Wittenberg A, Fanrong F (2009) Volcanic signals in oceans. J Geophys Res 114:D16104. doi:10.1029/2008JD011673

Stothers RB (1984) The great Tambora eruption and its aftermath. Science 224:1191–1198

Timmreck C, Lorenz SJ, Crowley TJ, Kinne S, Raddatz TJ, Thomas MA, Jungclaus JH (2009) Limited temperature response to the very large AD 1258 volcanic eruption. Geophys Res Lett 36: L21708. doi:10.1029/2009GL040083

Tsiropoula G (2003) Signatures of solar activity variability in meteorological parameters. J Atmos Sol Terr Phys 65:469–482

Wang R, Wang S, Fraedrich K (1991) An approach to reconstruction of temperature on seasonal basis using historical documents from China. Int J Climatol 11:381–392

Wang SW, Wen XY, Luo Y, Dong WJ, Zhao ZC, Yang B (2007) Reconstruction of temperature series of China for the last 1000 years. Chin Sci Bull 52:3272–3280

Wetzel P, Maier-Reimer E, Keenlyside N, Botzet M, Latif M, Jungclaus JH (2006) Effects of ocean biology on the penetrative radiation in a coupled climate model. J Climate 19:3973–3987

Yang B, Shi Y, Li HP (2001) Climatic variations in China over the last 2000 years. Chin Geogr Sci 11:97–103

Yang B, Bräuning A, Johnson KR, Shi YF (2002) General characteristics of temperature variation in China during the last two millennia. Geophys Res Lett 29:1324–1327. doi:10.1029/2001GL014485. Data from Yang et al. (2002) Temperature variation in China during the last two millennia. IGBP PAGES/World Data Center-A for Paleoclimatology Data Contribution Series #2002-061. NOAA/NGDC Paleoclimatology Program, Boulder CO, USA

Yang B, Bräuning A, Shi Y, Zhang J (2003) Temperature variations on the Tibetan Plateau over the last two millennia. Chin Sci Bull 48:1446–1450

Yang B, Wang JS, Bräuning A, Dong ZB, Esper J (2009) Late Holocene climatic and environmental changes in arid central Asia. Quatern Int 194:68–78

Zhang Q, Gemmer M, Chen J (2008) Climate change and flood/drought risk in the Yangtze delta, China, during the past millennium. Quatern Int 176–177:62–69

Zhang Y, Kong ZC, Yan S, Yang ZJ, Ni J (2009) "Medieval warm period" on the northern slope of central Tianshan mountains, Xinjiang, NW China. Geophys Res Lett 36:L11702

Zhu X, Fraedrich K, Blender R (2006) Variability regimes of simulated Atlantic MOC. Geophys Res Lett 33:L21603

Zorita E, von Storch H, González-Rouco F, Cubasch U, Luterbacher J, Legutke S, Fischer-Bruns I, Schlese U (2004) Climate evolution in the last five centuries simulated by an atmosphere–ocean model: global temperatures, the North Atlantic Oscillation and the Late Maunder Minimum. Meteorol Zeitschr 13:271–289